

Real-time, profile-corrected single snapshot imaging of optical properties

Martijn van de Giessen,^{1,2} Joseph P. Angelo,^{1,3} and Sylvain Gioux^{1,4,*}

¹Department of Medicine, Beth Israel Deaconess Medical Center, 330 Brookline Avenue, Boston, MA 02215, USA

²Division of Image Processing, Leiden University Medical Center, Albinusdreef 2, 2333 ZA, Leiden, The Netherlands

³Department of Biomedical Engineering, Boston University, 44 Cummington Street, Boston, MA 02215, USA

⁴ICube Laboratory, University of Strasbourg, 300 Bd S. Brant, 67412 Illkirch cedex, France

*sgيوخ@unistra.fr

Abstract: A novel acquisition and processing method that enables real-time, single snapshot of optical properties (SSOP) and 3-dimensional (3D) profile measurements in the spatial frequency domain is described. This method makes use of a dual sinusoidal wave projection pattern permitting to extract the DC and AC components in the frequency domain to recover optical properties as well as the phase for measuring the 3D profile. In this method, the 3D profile is used to correct for the effect of sample's height and angle and directly obtain profile-corrected absorption and reduced scattering maps from a single acquired image. In this manuscript, the 3D-SSOP method is described and validated on tissue-mimicking phantoms as well as *in vivo*, in comparison with the standard profile-corrected SFDI (3D-SFDI) method. On average, in comparison with 3D-SFDI method, the 3D-SSOP method allows to recover the profile within 1.2mm and profile-corrected optical properties within 12% for absorption and 6% for reduced scattering over a large field-of-view and in real-time.

©2015 Optical Society of America

OCIS codes: (170.3880) Medical and biological imaging; (110.2960) Image analysis.

References and links

1. S. Kukreti, A. E. Cerussi, W. Tanamai, D. Hsiang, B. J. Tromberg, and E. Gratton, "Characterization of metabolic differences between benign and malignant tumors: high-spectral-resolution diffuse optical spectroscopy," *Radiology* **254**(1), 277–284 (2010).
2. D. Roblyer, S. Ueda, A. Cerussi, W. Tanamai, A. Durkin, R. Mehta, D. Hsiang, J. A. Butler, C. McLaren, W. P. Chen, and B. Tromberg, "Optical imaging of breast cancer oxyhemoglobin flare correlates with neoadjuvant chemotherapy response one day after starting treatment," *Proc. Natl. Acad. Sci. U.S.A.* **108**(35), 14626–14631 (2011).
3. S. Gioux, H. S. Choi, and J. V. Frangioni, "Image-guided surgery using invisible near-infrared light: fundamentals of clinical translation," *Mol. Imaging* **9**(5), 237–255 (2010).
4. G. M. van Dam, G. Themelis, L. M. Crane, N. J. Harlaar, R. G. Pleijhuis, W. Kelder, A. Sarantopoulos, J. S. de Jong, H. J. Arts, A. G. van der Zee, J. Bart, P. S. Low, and V. Ntziachristos, "Intraoperative tumor-specific fluorescence imaging in ovarian cancer by folate receptor- α targeting: first in-human results," *Nat. Med.* **17**(10), 1315–1319 (2011).
5. D. J. Cuccia, F. Bevilacqua, A. J. Durkin, F. R. Ayers, and B. J. Tromberg, "Quantitation and mapping of tissue optical properties using modulated imaging," *J. Biomed. Opt.* **14**(2), 024012 (2009).
6. N. Dognitz and G. Wagnieres, "Determination of tissue optical properties by steady-state spatial frequency-domain reflectometry," *Lasers Med. Sci.* **13**, 55–65 (1998).
7. S. Gioux, A. Mazhar, B. T. Lee, S. J. Lin, A. M. Tobias, D. J. Cuccia, A. Stockdale, R. Oketokoun, Y. Ashitate, E. Kelly, M. Weinmann, N. J. Durr, L. A. Moffitt, A. J. Durkin, B. J. Tromberg, and J. V. Frangioni, "First-in-human pilot study of a spatial frequency domain oxygenation imaging system," *J. Biomed. Opt.* **16**(8), 086015 (2011).
8. A. Yafi, T. S. Vetter, T. Scholz, S. Patel, R. B. Saager, D. J. Cuccia, G. R. Evans, and A. J. Durkin, "Postoperative quantitative assessment of reconstructive tissue status in a cutaneous flap model using spatial frequency domain imaging," *Plast. Reconstr. Surg.* **127**(1), 117–130 (2011).
9. J. T. Nguyen, S. J. Lin, A. M. Tobias, S. Gioux, A. Mazhar, D. J. Cuccia, Y. Ashitate, A. Stockdale, R. Oketokoun, N. J. Durr, L. A. Moffitt, A. J. Durkin, B. J. Tromberg, J. V. Frangioni, and B. T. Lee, "A novel pilot

- study using spatial frequency domain imaging to assess oxygenation of perforator flaps during reconstructive breast surgery,” *Ann. Plast. Surg.* **71**(3), 308–315 (2013).
10. A. M. Laughney, V. Krishnaswamy, E. J. Rizzo, M. C. Schwab, R. J. Barth, Jr., D. J. Cuccia, B. J. Tromberg, K. D. Paulsen, B. W. Pogue, and W. A. Wells, “Spectral discrimination of breast pathologies in situ using spatial frequency domain imaging,” *Breast Cancer Res.* **15**(4), R61 (2013).
 11. A. Ponticorvo, D. M. Burmeister, B. Yang, B. Choi, R. J. Christy, and A. J. Durkin, “Quantitative assessment of graded burn wounds in a porcine model using spatial frequency domain imaging (SFDI) and laser speckle imaging (LSI),” *Biomed. Opt. Express* **5**(10), 3467–3481 (2014).
 12. D. J. Rohrbach, D. Muffoletto, J. Huihui, R. Saager, K. Keymel, A. Paquette, J. Morgan, N. Zeitouni, and U. Sunar, “Preoperative mapping of nonmelanoma skin cancer using spatial frequency domain and ultrasound imaging,” *Acad. Radiol.* **21**(2), 263–270 (2014).
 13. T. E. Travis, P. Ghassemi, J. C. Ramella-Roman, N. J. Prindeze, D. W. Paul, L. T. Moffatt, M. H. Jordan, and J. W. Shupp, “A multimodal assessment of melanin and melanocyte activity in abnormally pigmented hypertrophic scar,” *J. Burn Care Res.* **36**(1), 77–86 (2015).
 14. K. P. Nadeau, A. J. Durkin, and B. J. Tromberg, “Advanced demodulation technique for the extraction of tissue optical properties and structural orientation contrast in the spatial frequency domain,” *J. Biomed. Opt.* **19**(5), 056013 (2014).
 15. J. Vervandier and S. Gioux, “Single snapshot imaging of optical properties,” *Biomed. Opt. Express* **4**(12), 2938–2944 (2013).
 16. S. Gioux, A. Mazhar, D. J. Cuccia, A. J. Durkin, B. J. Tromberg, and J. V. Frangioni, “Three-dimensional surface profile intensity correction for spatially modulated imaging,” *J. Biomed. Opt.* **14**(3), 034045 (2009).
 17. T. J. Farrell, M. S. Patterson, and B. Wilson, “A diffusion theory model of spatially resolved, steady-state diffuse reflectance for the noninvasive determination of tissue optical properties in vivo,” *Med. Phys.* **19**(4), 879–888 (1992).
 18. M. A. Neil, R. Juskaitis, and T. Wilson, “Method of obtaining optical sectioning by using structured light in a conventional microscope,” *Opt. Lett.* **22**(24), 1905–1907 (1997).
 19. T. A. Erickson, A. Mazhar, D. Cuccia, A. J. Durkin, and J. W. Tunnell, “Lookup-table method for imaging optical properties with structured illumination beyond the diffusion theory regime,” *J. Biomed. Opt.* **15**(3), 036013 (2010).
 20. G. Indebetouw, “Profile measurement using projection of running fringes,” *Appl. Opt.* **17**(18), 2930–2933 (1978).
 21. V. Srinivasan, H. C. Liu, and M. Halioua, “Automated phase-measuring profilometry of 3-D diffuse objects,” *Appl. Opt.* **23**(18), 3105 (1984).
 22. M. Takeda and K. Mutoh, “Fourier transform profilometry for the automatic measurement of 3-D object shapes,” *Appl. Opt.* **22**(24), 3977 (1983).
 23. C. D’Andrea, N. Ducros, A. Bassi, S. Arridge, and G. Valentini, “Fast 3D optical reconstruction in turbid media using spatially modulated light,” *Biomed. Opt. Express* **1**(2), 471–481 (2010).
 24. S. Bélanger, M. Abran, X. Intes, C. Casanova, and F. Lesage, “Real-time diffuse optical tomography based on structured illumination,” *J. Biomed. Opt.* **15**(1), 016006 (2010).
 25. W. Zhou and X. Su, “A direct mapping algorithm for phase-measuring profilometry,” *J. Mod. Opt.* **41**(1), 89–94 (1994).
 26. F. Ayers, A. Grant, D. Kuo, D. J. Cuccia, and A. J. Durkin, “Fabrication and characterization of silicone-based tissue phantoms with tunable optical properties in the visible and near infrared domain,” in *Proc. SPIE*, (2008), 6870E.
 27. F. Bevilacqua, A. J. Berger, A. E. Cerussi, D. Jakubowski, and B. J. Tromberg, “Broadband absorption spectroscopy in turbid media by combined frequency-domain and steady-state methods,” *Appl. Opt.* **39**(34), 6498–6507 (2000).

1. Introduction

Over the last few years, sub-surface diffuse optical imaging has been making constant progress towards reaching the bedside, in particular in the fields of functional point measurement [1, 2] and wide-field surgical guidance [3, 4]. However, providing real-time quantitative sub-surface images remains a significant challenge that has been strongly limiting diffuse optical imaging in being more widely applied in the clinic. Recent developments in Spatial Frequency Domain Imaging (SFDI) have shed hopes in solving this fundamental issue [5, 6]. This method relies on the analysis of the spatial frequency response of turbid media to structured illumination (i.e. stripes of light), allowing the characterization of an entire field-of-view at once (i.e. in a multipixel approach). SFDI has shown significant promise in performing wide-field surgical guidance and specimen examination, both in animals and in humans, *ex vivo* and *in vivo* [7–13].

Despite its capabilities of analyzing full fields-of-view at once, traditional SFDI acquisitions have been limited to phase shifting approaches to extract the tissue response to structured illumination, impairing its capabilities to perform in real time. While a minimum of 3 phases is required to extract the AC and DC components of a sinewave [5, 6], a total of 6 images are commonly used to extract optical properties (absorption and reduced scattering), 3 phases at 2 spatial frequencies, with this number increasing to 9 images when performing simultaneous profile acquisition to correct for the effects of the sample distance and profile.

Efforts are currently being made to find alternative demodulation techniques to reduce the acquisition time in the spatial frequency domain. Nadeau et al. introduced a two-dimensional Hilbert transform method requiring only 2 images to extract the necessary information for deducting optical properties [14]. While much faster than the traditional 3-phases approach, this method still uses two sequential images, and necessitates expensive and complex instrumentation to synchronize the projection (DMD projector, or sequential projection slides with a rotating wheel) with camera acquisition to perform at a real-time level. Our group recently introduced Single Snapshot of Optical Properties (SSOP), a method working entirely in the frequency domain that necessitates the acquisition of a single image to extract the optical properties [15]. While very rapid and inexpensive (a single sinusoidal pattern printed on a transparency film is necessary), this method suffers from a degraded image quality due to the single phase acquisition and spatial frequency filtering.

While these recent advances improve the capabilities of SFDI for forming quantitative images rapidly over a large field-of-view, none is taking into account the 3D-surface profile of the sample, a major source of error using non-contact imaging techniques. As part of previous work, we introduced a method capable to acquire both the profile and optical properties sequentially in the spatial frequency domain, and using the 3D-profile information to correct for the effects of sample-to-imaging device distance and of sample's surface angle [16]. Not correcting for these effects can lead to very strong variations in optical properties, 10% errors on average per cm, and 86% for a 40 degree surface angle, preventing the use of SFDI during many clinical scenarios [16].

In this work, we present a novel acquisition and processing method that recovers both optical properties and surface profile from a single snapshot acquisition. This method is based on the previously developed Single Snapshot of Optical Properties (SSOP) method, but with the difference that both the phase and the amplitude modulation of a 2-dimensional sinusoidal intensity wave are recovered from a single projection. The method was validated on tissue mimicking phantoms and *in vivo*. Tissue mimicking phantoms with known absorption (μ_a) and reduced scattering (μ_s') coefficients were imaged using the single acquisition method and compared to the original 3-phase SFDI acquisition method. Finally, a demonstration of real-time acquisition using 3D-SSOP was performed on both a hemispherical tissue mimicking phantoms and on a human hand. Together, this study lays the foundation for the development of real-time quantitative sub-surface imaging for the clinic.

2. Material and methods

2.1. Spatial frequency domain imaging (SFDI)

Spatial frequency domain imaging (SFDI) has been described extensively in the literature [5] and will be only briefly summarized here. Analogous to the temporal point-spread function (t-PSF) response to a pulse illumination in time-domain, a point source that illuminates tissue induces a diffuse reflectance with a spatial point spread function (s-PSF). The shape of the spatial decay of the s-PSF is characteristic of the sub-surface optical properties of the tissue [17]. Just as temporal frequency-domain measurements acquire as a function of temporal frequency the t-MTF (Modulation Transfer Function, the t-PSF Fourier equivalent), SFDI acquires the s-MTF as a function of spatial frequency by projecting a wide 1D intensity sinusoidal wave on the tissue [6].

The medium s-MTF is represented by the diffuse reflectance R_d measured at a location x and spatial frequency f_x . The diffuse reflectance R_d of the medium (here considered homogeneous and with a semi-infinite geometry) can be modeled in various ways using the diffusion approximation to the radiative transport equation or Monte-Carlo [5]. On the other end, instrumentally, the diffuse reflectance is measured by extracting the amplitude modulation $M(x, f_x)$ from a projected intensity sinusoidal wave. Once the diffuse reflectance has been measured, solving the inverse problem allows the recovery of the optical properties of the medium.

Relevant to this work, the acquisition of the amplitude modulation of the projected sinusoidal wave traditionally relies on a 3-phases demodulation technique [18]. The intensity I of a sinusoidal wave as a function of x , at a spatial frequency f_x and phase Φ_i projected on the medium is acquired on the camera as:

$$I_i(x, f_x) = M(x, f_x) \cos(f_x \cdot x + \phi_i) + I_{DC}(x) \quad (1)$$

where $M(x, f_x)$ is the amplitude modulation, and I_{DC} the DC component. $M(x, f_x)$ is obtained by projecting three sequential sinusoidal waves with phases $\Phi_{i=1-3} = [0^\circ, 120^\circ, 240^\circ]$:

$$M(x, f_x) = \frac{\sqrt{2 \left\{ [I_1(x, f_x) - I_2(x, f_x)]^2 + [I_2(x, f_x) - I_3(x, f_x)]^2 + [I_3(x, f_x) - I_1(x, f_x)]^2 \right\}}}{3} \quad (2)$$

The amplitude modulation $M(x, f_x)$ can be related to the measured diffuse reflectance $R_d(x, f_x)$:

$$M(x, f_x) = I_0 \cdot MTF_{sys}(x, f_x) \cdot R_d(x, f_x) \quad (3)$$

with I_0 the source intensity and $MTF_{sys}(x, f_x)$ the amplitude modulation of the optical system (e.g. lenses). Finally, the medium diffuse reflectance is obtained by using a calibration reference with known optical properties:

$$R_d(x, f_x) = \frac{M(x, f_x)}{M_{ref}(x, f_x)} \cdot R_{dref}(x, f_x) \quad (4)$$

where $M_{ref}(x, f_x)$ is measured on the calibration reference, and $R_{dref}(x, f_x)$, modeled based on the known optical properties of the medium

In the traditional “fast” acquisition implementation, only two spatial frequencies are necessary to extract the medium optical properties [5]. One low frequency, typically $f_x = 0 \text{ mm}^{-1}$, called DC here, is sensitive to changes in both reduced scattering and absorption; while another high frequency, typically $f_x = 0.2 \text{ mm}^{-1}$, called AC here, is mainly sensitive to changes in reduced scattering [5]. This property allows to precompute solutions to the inverse problem into a lookup table using Monte-Carlo, where a unique set of optical properties corresponds to a unique set of diffuse reflectance values [5, 19], allowing rapid extraction of optical properties from the measurement of a DC and an AC component.

2.2. Profile-correction for SFDI

SFDI, as most quantitative optical imaging methods, suffers from assumptions and imperfections, including modeling errors (medium is not homogeneous or semi-infinite) and instrumental errors (medium is not flat and at a variable distance). In this work, we address the errors related to the non-flatness and distance variations of the medium. In particular, in clinical practice, the assumption of a flat sample is challenging to satisfy, leading to calibration errors due to 1) variations in distance between the imaging system and the sample, and 2) the sample’s local surface angle. Using a multi-height calibration method along with a Lambertian model for the reemitted light intensity from diffusive surfaces, the local intensity of the collected light can be corrected for these two effects. Using this approach, optical

properties can be corrected for the effect of the sample's distance and surface profile, as evidenced in the difference between corrected and uncorrected optical properties maps [16].

In order to simultaneously perform optical properties and surface height measurements using structured illumination (i.e. patterns of light), the patterns are projected at an angle compared to the collection axis. As explained in details previously [16], and illustrated in Fig. 1, optical properties are obtained by projecting sinusoidal intensity patterns that are parallel to the plane spanned by the projector and optical collection axes. Such a projection ensures that the phase of the projected sinusoidal wave is insensitive to height variations (called here profile-insensitive patterns). Following optical properties acquisition, the surface profile is obtained through phase profilometry. Contrary to the pattern orientation used to obtain optical properties, the projected profilometry fringes need to be maximally sensitive to height variations and are projected perpendicular to the plane formed by the projection and collection axes (called here profile-sensitive patterns). The height-dependent phase is then obtained by demodulating a three phase acquisition, called phase-shifting profilometry [20, 21]. Finally, the sample distance and angle are used to correct the intensity of the SFDI acquisition at each pixel. This approach has been validated and translated to the clinic [7].

Alternatively, using Fourier transform profilometry, a single image can be used to determine the height dependent phase of a projected profilometry fringe [22]. Because it relies on a single projection pattern, and therefore allows real-time measurements, this approach is taken in this work. Here the intensity variations due to the projected fringes are assumed to dominate intensity variations from tissue reflectivity in the spectral band around the projected carrier spatial frequency f_y . Taking the 1D Fourier transform in the image direction along the projected profilometry fringes enables separation of the profilometry information from slower varying intensity changes. Through the selection of only the positive sideband around f_y and applying the inverse 1D Fourier transform, a complex signal is obtained that contains the local phases ϕ_y . The phase difference $\Delta\phi$ between ϕ_y and the local phases ϕ_0 in a reference plane is directly related to the distance between camera and tissue.

2.3. Single snapshot of optical properties (SSOP)

We previously developed an acquisition and demodulation method, called Single Snapshot of Optical Properties (SSOP), capable of extracting optical properties in the spatial frequency domain from a single acquired image. SSOP works by projecting a single sinusoidal pattern onto the specimen and relies on processing entirely in the frequency domain to extract the DC and AC components (i.e. 2 spatial frequencies) that are used to calculate the specimen's optical properties [15]. Briefly, a single sinusoidal pattern is projected onto the field-of-view and analyzed in the Fourier domain in a line-by-line 1D approach. The DC and AC components are extracted by filtering the DC component (ideal rectangular filter $[0; f_c]$), and the AC component (ideal rectangular filter $[f_c; f_{\max}]$), f_c being optimized to minimize the cross talk between the two components, and f_{\max} being the maximal spatial frequency. These components are then used to obtain the diffuse reflectance at these two spatial frequencies and in a pre-computed lookup table to extract the optical properties.

2.4. Simultaneous imaging of optical properties and 3-D profile (3D-SSOP)

While prior work in tomography has already shown the use of multiple patterns and processing in the 2D-Fourier space [23, 24], this concept has not been described for simultaneous surface profile and sub-surface optical properties imaging. In this work, we propose to extend these principles to acquire simultaneously both optical properties and surface profile in real-time, and to directly obtain profile-corrected optical properties maps from a single image. For this purpose, a pattern containing two superimposed sinusoidal waves, orthogonal to each other, are projected onto the specimen.

$$I(x, y, f_x, f_y) = \frac{1}{2} + \frac{1}{4} \left[\cos(f_x \cdot x + \phi_x) + \cos(f_y \cdot y + \phi_y) \right] \quad (5)$$

Specifically, one pattern (along the x direction) will be used for optical properties processing (similarly to standard SSOP) and the other (along the y direction) for extracting the specimen surface profile [16]. As illustrated in Fig. 1, by projecting a dual sinusoidal wave pattern, one can gather information regarding both profile-sensitive pattern orientation (horizontal in this case) and optical properties, profile-insensitive pattern orientation (vertical in this case). Note that the profile-sensitive patterns are also sensitive to optical properties. However, the sinusoidal wave phase variations renders the amplitude modulation extraction challenging. In essence, the profile sensitive patterns are used to extract the phase of each pixel in the image that can in turn be used to deduce each pixel's height [25]. Following this step, the profile insensitive patterns are used to extract the AC and DC components of the image, similarly to standard SSOP. Finally, the height information is used correct for both height and angle effects, and optical properties extracted [16].

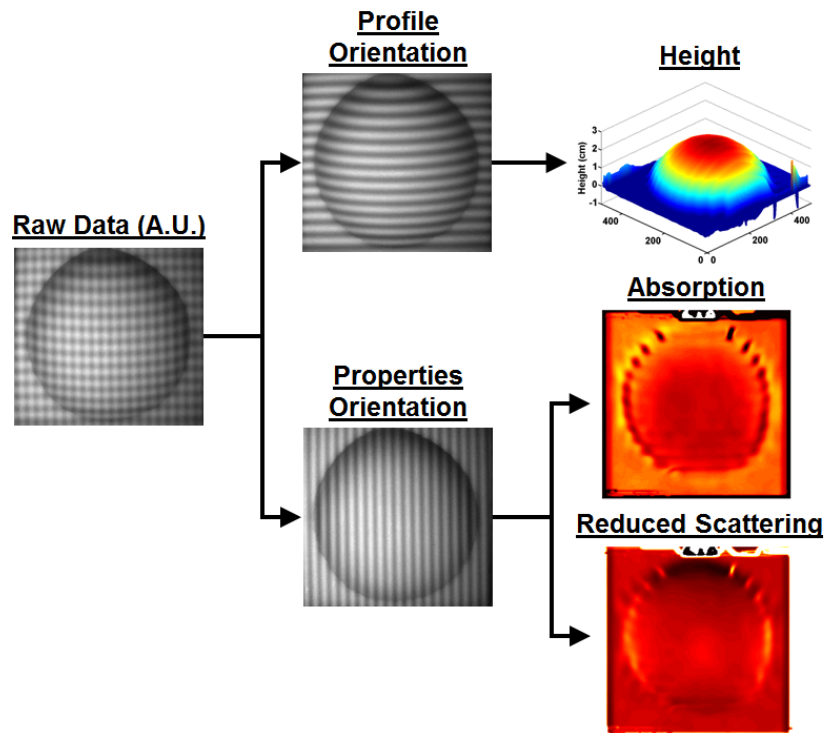


Fig. 1. 3-D Single Snapshot of Optical Properties. A dual sinusoidal wave is projected, one wave being sensitive to the specimen's optical properties and the other to the specimen's profile. AC & DC components as well as phase are extracted (not shown here) leading to profile, absorption and reduced scattering.

More precisely, the AC and DC components as well as the phase for profilometry are estimated in frequency space. In this space, the optical properties sinewave [properties orientation in Fig. 1] exhibits a narrow band in one direction and the profilometry sinewave [profile orientation in Fig. 1] a narrow band in a second direction, perpendicular to the first one [see Fig. 2(c)]. The orthogonality in the Fourier domain and clear detectability of frequency bands enables separation of the AC and DC components, as well as the phase for Fourier transform profilometry.

In 3D-SSOP each image is analyzed according to the schematics in Fig. 2. After acquisition, each frame is expanded using mirrored images to minimize artifacts due to

discontinuities at the image edges [Fig. 2(b)]. The expanded image is transformed to the frequency domain with a two-dimensional Fourier transform [Fig. 2(c)]. The DC and AC components are obtained by filtering in the frequency domain with blocking rectangular filters ($[f_{xDClow}; f_{xDChigh}] \& [f_{yDClow}; f_{yDChigh}]$) and ($[f_{xAClow}; f_{xAChigh}] \& [f_{yAClow}; f_{yAChigh}]$), respectively, as shown in Figs. 2(d) and 2(e). The phase is obtained by filtering in the frequency domain with a blocking rectangular filter ($[f_{xPHIlow}; f_{xPHIhigh}] \& [f_{yPHIlow}; f_{yPHIhigh}]$), as shown in Fig. 2(f). For simplicity, the filters used in this work were ideal rectangular filters in the frequency domain, i.e. sinc filters in the real domain. Note that these filters have cutoff frequencies in 2 dimensions (f_x and f_y) since this method is described in the 2D Fourier space. These filters are designed to select the appropriate frequency bands, while minimizing the formation of artifacts near discontinuities in the images. The latter is achieved by preserving the high frequency information in each of the filters. The bands that cover the projected waves are centered on the projected frequency. In this work, the band centers are estimated by peak detection in a 2D Fourier transform of a flat calibration image. Depending on the acquisition geometry and the expected variation in distance to sample, one could re-estimate the bands from each frame. The widths of the bands are user-determined and depend on the accuracy of the projected sine waves and on the expected steepness of ramps in the field-of-view.

After filtering, an inverse two-dimensional Fourier transform is applied to each of the filtered frequency domain images. The DC component is a direct result of the inverse two-dimensional Fourier transform [Fig. 2(g)]. The inverse Fourier transformed images for the AC and phase components are obtained by applying an additional Hilbert transform [Figs. 2(h) and 2(i), respectively]. The final images are obtained by selecting the central portion of the expanded frames.

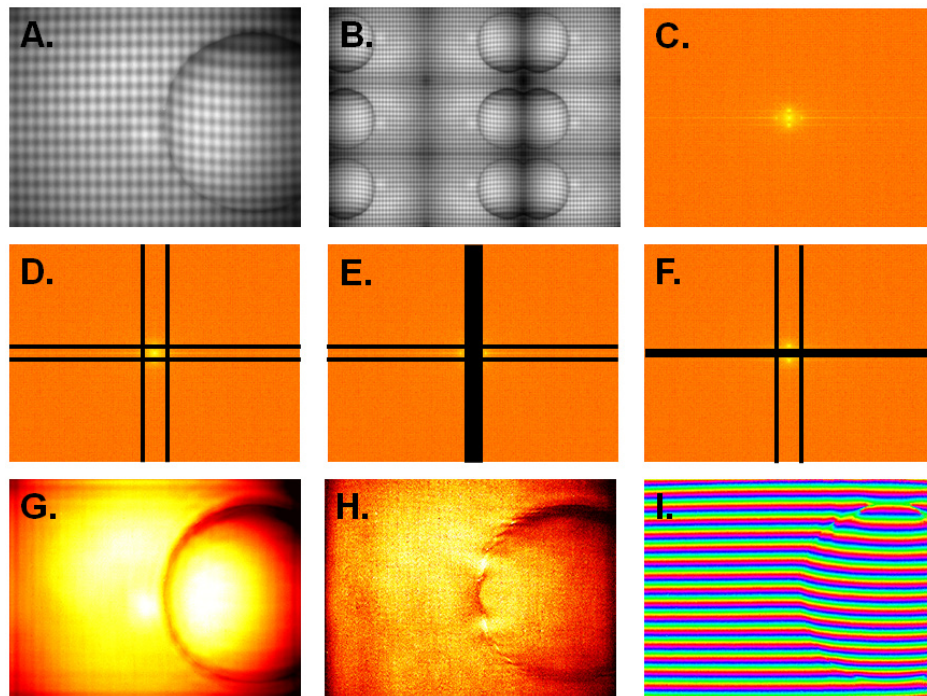


Fig. 2. Data processing for 3-D Single Snapshot of Optical Properties. The acquired image (A) is expanded by mirroring (B) and a 2D Fourier transform performed (C). Filters (D, E and F) are then used to isolate the DC component (G), the AC component (H) and the phase (I), respectively.

2.5 Instrumental setup

Samples were acquired on a custom-made instrumental setup comprised of a projector, a collection objective lens and a monochrome camera. The projector consisted of a digital micromirror device (DMD; GFM, Berlin, Germany), fiber-coupled coupled to a 670nm laser diode (LDX Optronics, Maryville, Tennessee) and projecting pre-programmed patterns using MATLAB (Mathworks, Natick, MA). A first linear polarizer (Moxtek, Inc., Orem, Utah) was placed in front of the projector lens (NIR S2 + ; Carl Zeiss, Oberkochen, Germany). Images were collected through a custom imaging system (Qioptic, Waltham, MA) and imaged onto a monochrome camera (ORCA, Hamamatsu, Bridgewater, New Jersey). A second linear polarizer was placed in front of the collection objective lens, cross-polarized with respect to the first polarizer, to preferentially collect light that has diffused inside the medium and minimize the influence of specular reflections. Software was written in C#/C++ for controlling acquisitions (projector and cameras) and recording data. Data was post-processed using custom-developed MATLAB code. This setup and the associated processing were previously validated during several experiments, including a clinical trial [16].

2.6. Calibration

Spatial Frequency Domain Imaging necessitates a calibration measurement [5]. Our imaging setup was calibrated using a flat, homogeneous, tissue-mimicking phantom of $96 \times 96 \times 20$ mm with known optical properties. All phantoms consisted of polydimethylsiloxane with India ink as absorber and TiO₂ as scattering agent [26]. The calibration phantom spectral absorption and reduced scattering coefficients were verified with two-distance, multifrequency Frequency Domain Photon Migration (FDPM) independent measurements [27]. This calibration phantom was then used as ground-truth to deduct other phantoms optical properties. In addition, since 3D profile correction is performed, the height-dependent frequency response was calibrated by acquiring our calibration phantom at 6 heights with 1 cm steps.

2.7. Experiments

Three experiments were performed to compare the accuracy and precision of the proposed 3D-SSOP method with standard three-phase modulation and profilometry-corrected SFDI (3D-SFDI). All images have been acquired a 670nm and at a spatial frequency of 0.2mm^{-1} for optical properties calculation and of 0.15mm^{-1} for phase extraction. Cutoff frequencies for the blocking filters were set at (in mm^{-1}) - see Fig. 2:

- For the DC component: $f_{\text{DClow}} = 0.16$; $f_{\text{DChigh}} = 0.24$; $f_{\text{yDClow}} = 0.105$; $f_{\text{yDChigh}} = 0.195$
- For the AC component: $f_{\text{xAClow}} = 0$; $f_{\text{xACHigh}} = 0.16$; $f_{\text{yAClow}} = 0.105$; $f_{\text{yACHigh}} = 0.195$
- For the phase component: $f_{\text{xPHIlow}} = 0.16$; $f_{\text{xPHIhigh}} = 0.24$; $f_{\text{yPHIlow}} = 0$; $f_{\text{yPHIhigh}} = 0.105$

Flat homogeneous phantom: In this experiment, height and optical properties were recovered from a tissue-mimicking phantom with known optical properties, imaged at six heights with steps of 1cm. Using titanium oxide (TiO₂) as a scattering agent and India ink as absorbing agent, optical properties were set at 0.036mm^{-1} for absorption (μ_a) and 0.97mm^{-1} for reduced scattering (μ_s'). Height and profile-corrected optical properties maps were extracted using both methods and compared with non-profile-corrected maps using SFDI.

Hemispheric homogeneous phantom: In this experiment a hemispheric tissue-mimicking phantom on top of a flat homogeneous tissue-mimicking phantom having the same optical properties ($\mu_a = 0.023\text{mm}^{-1}$ and $\mu_s' = 0.97\text{mm}^{-1}$) were imaged with both methods. Height and profile corrected optical properties maps were extracted and their percentage difference assessed. Finally a movie was captured where the phantom is imaged in real-time using the 3D-SSOP method.

In-vivo measurement: A hand movie was captured where the hand is imaged in real-time for both height and profile-corrected optical properties using the 3D-SSOP method.

3. Results

3.1. Flat homogeneous phantom

The results from the flat homogeneous phantoms experiments are shown in Fig. 3. A comparison of profile corrected maps of absorption processed either with profile-corrected SFDI (3D-SFDI) or 3D-SSOP is plotted in 3D in Figs. 3(a) and 3(b). One can notice a good agreement between the two methods, both in 3D profile and in absorption values. This agreement is quantified and confirmed both in height [plot shown in Fig. 3(c)] and in optical properties [absorption shown in Fig. 3(d) and reduced scattering shown in Fig. 3(e)]. Both 3D-SFDI and 3D-SSOP evidenced accurate and precise height estimation, on average within 1.1mm of the expected height and with an average standard deviation of 0.7mm. Similarly both methods were able to extract and correct optical properties for all sample heights, within 1.25% of the expected value (0.0005 mm^{-1} average absolute difference), and with 3.1% coefficient of variation for absorption, and 1.1% of the expected value (0.01 mm^{-1} average absolute difference), and with 1.6% coefficient of variation for reduced scattering. Note the extent of the correction necessary to account for the change in height of the sample.

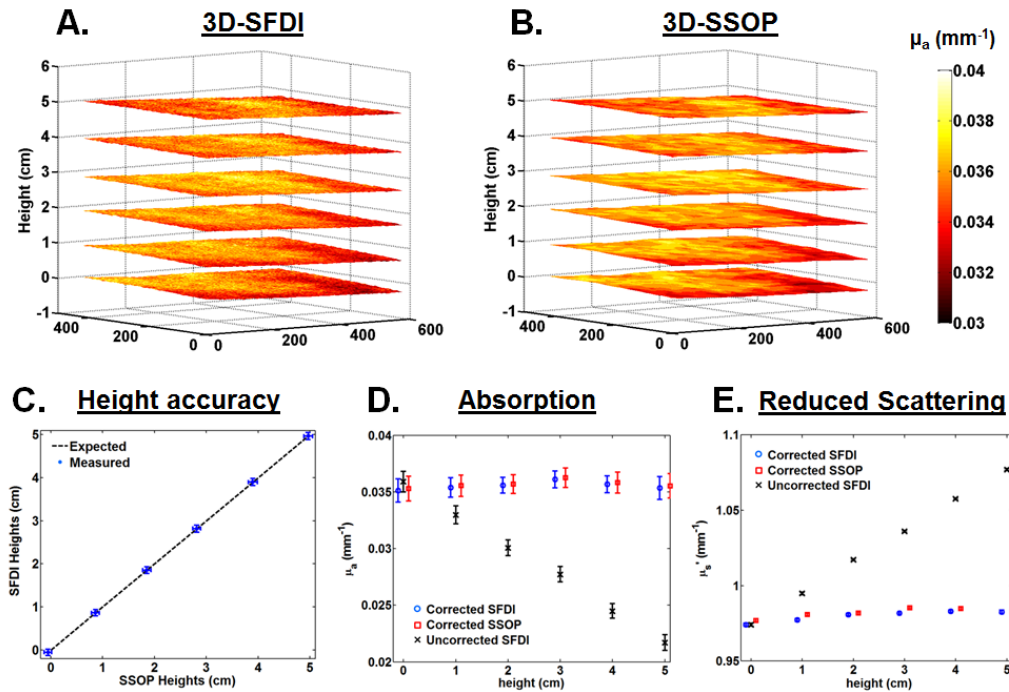


Fig. 3. Flat homogeneous phantom measurements. 3D-SFDI and 3D-SSOP methods were used to acquire and process a set of homogeneous phantoms at different heights (A and B, respectively). Notice the good agreement in heights (C), and in profile-corrected values for absorption (D) and reduced scattering (E).

3.2. Hemispheric homogeneous phantom

The results from the hemispherical phantom measurements are shown in Fig. 4. As expected from a single image measurement, the 3D-SSOP maps exhibit artifacts on the edges, as well as noise due to the variation in angle and height of the surface (themselves due to noise in the 3D profile data). However, on average the novel method performs fairly well, within 1.2mm

of the 3D-SFDI data for height with a 0.3mm standard variation, 12% for absorption (0.0055 mm^{-1} average absolute difference) with a 4.2% coefficient of variation and 6.1% for reduced scattering (0.097 mm^{-1} average absolute difference) with a 1.7% coefficient of variation (*note: errors are calculated from the absolute difference between the two methods, not the relative difference that would artificially give a lower error*).

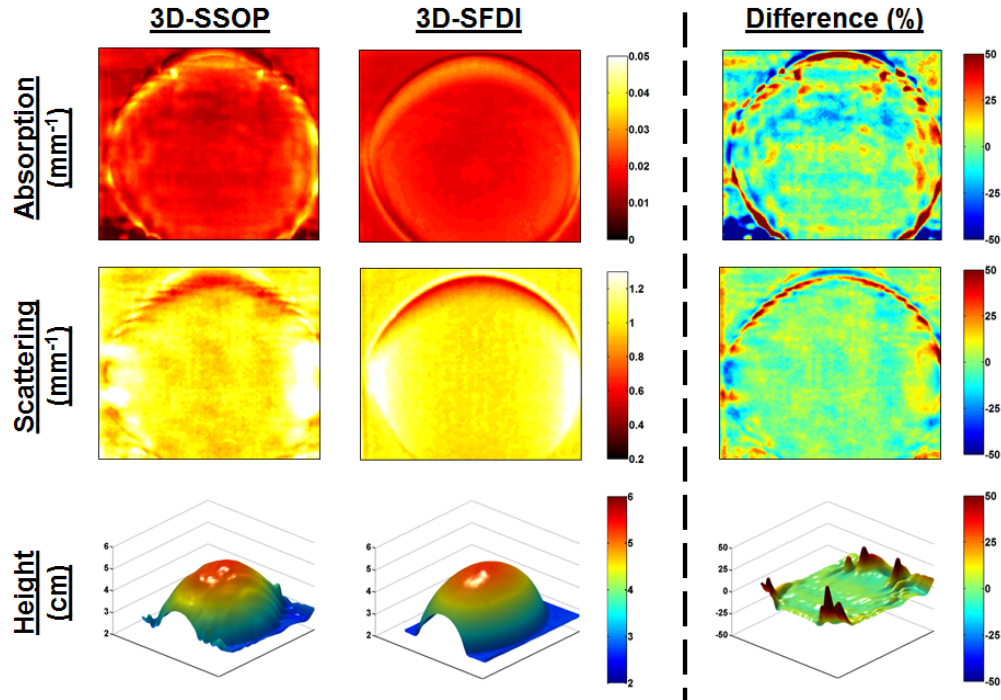


Fig. 4. Hemispheric phantom measurements. 3D-SFDI and 3D-SSOP methods were used to acquire and process a hemispheric homogeneous phantom. Notice the good agreement in heights, as well as in profile corrected values for absorption and reduced scattering.

To illustrate the advantage of this new method to provide real-time quantitative measurements of optical properties in realistic conditions, i.e. with profile-correction, we included a movie of the hemispheric phantom moving in space. Acquisition time was set at 220ms, giving a frame rate of 4.5 frames per second. Are shown in Fig. 5: the raw data (top, left), the 3D profile data (top, right), and the optical properties (absorption: bottom, left; reduced scattering: bottom, right). Note the quality of the 3D profile data as well as the quantitative values of optical properties over the image while the specimen moves.

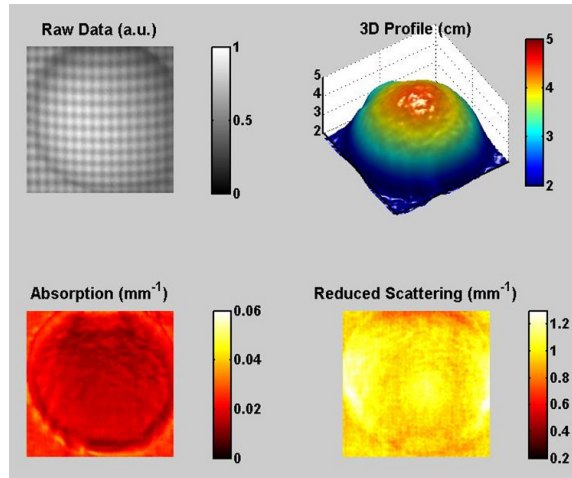


Fig. 5. Frame from the hemispheric phantom movie. A movie of a homogeneous hemispheric phantom was acquired with the 3D-SSOP method. Raw data (top, left), 3D profile (top, right), profile-corrected absorption (bottom, left) and reduced scattering (bottom, right) are shown. See [Visualization 1](#).

3.3. *In-vivo* measurement

To validate the novel method capability for providing real-time quantitative optical properties images with profile correction *in vivo*, we acquired a movie of a hand moving while performing a continuous 3D-SSOP measurement. Acquisition time was set at 150 ms, giving a frame rate of 6.7 frames per second. Are shown in Fig. 6: the raw data (top, left), the 3D profile data (top, right), and the optical properties (absorption: bottom, left; reduced scattering: bottom, right). Note the quality of the 3D profile data as well as the quantitative values of optical properties over the image while the specimen moves.

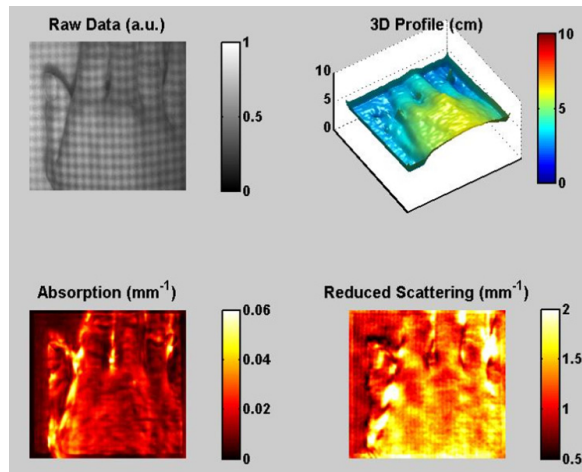


Fig. 6. Frame from the *in-vivo* hand movie. A movie of a hand was acquired with the 3D-SSOP method. Raw data (top, left), 3D profile (top, right), profile-corrected absorption (bottom, left) and reduced scattering (bottom, right) are shown. See [Visualization 2](#).

4. Discussion

In this work we described and validated a novel method called 3D-SSOP that is capable of acquiring and processing profile-corrected optical properties maps from a diffuse medium. This method relies on projecting a dual sinewave and extracting orthogonally in the frequency

domain the DC and AC components necessary to calculate optical properties, and the phase necessary to deduce the sample's 3D profile. The 3D profile is then used to correct for errors due to the mismatch between calibration and sample surface profile, and to obtain profile-corrected optical properties from a single acquired image. It is important to highlight that this method enables quantitative optical imaging over a large field of view ($>100\text{cm}^2$) in real-time and in realistic conditions for future clinical use.

This method offers two important improvements over the previous SSOP method. First, it is capable of simultaneous profile and optical properties measurements, which enables a broad range of applications compared to current methods, such as standard SSOP, that suffers from severe quantitative errors due to sample's height and angle. Second, it introduces SSOP processing in the 2D Fourier space, which along with a novel fast 2D lookup table, enables real-time processing with an average image processing time of less than 125ms. Since this novel fast 2D lookup table is independent to the work presented in this article, it will be the subject of another publication. It is important to note that 3D-SSOP truly enables real-time imaging through both acquisition and processing. Such a feature is highly desirable to reach future clinical use.

However, this method does introduce supplementary artifacts. On top of the image degradation caused by a single phase projection, and therefore energy spectrum losses, the phase itself is noisy, leading to artifacts that are visible in the sample's 3D profile. In turn these artifacts are visible in the optical properties maps, in particular through the surface angle correction that amplifies the profile noise. This effect is noticeable in the hemispheric homogenous phantom results, where the error in absorption reaches 12% difference relative to the expected value. This value is slightly above the 10% relative difference that is typically considered acceptable for wide-field diffuse optical imaging methods. Several solutions are currently being investigated to increase the resolution of SSOP and the precision of the reconstructed 3D profile and therefore reduce the profile correction noise.

Finally, this method remains to be integrated within a preclinical imaging setup and tested through preclinical experiments towards enabling real-time tissue endogenous chromophore quantitative imaging. The possibilities offered by such a system are particularly interesting in surgery where feedback regarding the status and function of tissue is required in real-time.

5. Conclusion

The 3D-SSOP method allows for real-time imaging of profile-corrected tissue properties from a single acquired image. In this article, we presented the principles of this method and evaluated its performance onto tissue mimicking phantoms and *in vivo*, in comparison with standard profile-corrected Spatial Frequency Domain Imaging (3D-SFDI). Overall, the 3D-SSOP method performs similarly to the 3D-SFDI method, with some image degradation but with the unique property of enabling real-time profile-corrected quantitative optical imaging. This work lays the foundation for the investigation of real-time surgical image-guidance using endogenous contrast.

Acknowledgments

The authors would like to thank Florin Neacsu for assistance with the SFDI acquisition software. This work was supported by NIH/NIDDK Award Number K01-DK-093603, NIH/NIDDK Award Number F31-DK-105839, by the Dutch Center for Translational Molecular Imaging (MUSiS), and by ICube.